Macromolecules

ARTICLE

pubs.acs.org/Macromolecules

Directing Thermoplastic Elastomer Microdomain Parallel to Fiber Axis: A Model Case of SEBS with Benzoxazine through $\pi-\pi$ Stacking

Wonchalerm Rungswang,[†] Masaya Kotaki,[§,*] Takuma Shimojima,[⊥] Go Kimura,[⊥] Shinichi Sakurai,[⊥,*] and Suwabun Chirachanchai[†,‡,*]

[†]The Petroleum and Petrochemical College, Chulalongkorn University, Soi Chula 12, Phyathai Road, Pathumwan, Bangkok, 10330 Thailand

[‡]Center for Petroleum, Petrochemicals, and Advanced Materials, Chulalongkorn University, Bangkok, 10330, Thailand

[§]Department of Advanced Fibro-science, Kyoto Institute of Technology, Matsugasaki, Sakyo-ku, Kyoto 606-8585, Japan

[⊥]Department of Biobased Materials Science, Graduate School of Science and Technology, Kyoto Institute of Technology, Matsugasaki, Sakyo-ku, Kyoto 606-8585, Japan

ABSTRACT: In our previous work, we revealed for the first time the existence of ordered-lamellar microdomains in thermoplastic elastomer based on the case study of an as-spun electrospun polystyrene-*b*-poly(ethylene-*co*-1-butene)-*b*-polystyrene triblock copolymer (SEBS), and also demonstrated how the extensional force initiated a certain level of lamellar-microdomain orientation. The present work shows the approach to direct lamellar-microdomain orientation to be parallel to the fiber axis by simply initiating a specific molecular interaction among thermoplastic elastomer chains. The blend system of SEBS and bisphenol A based benzoxazine monomer (BZ) forms $\pi-\pi$ interaction as confirmed by the nuclear overhauser effect in the nuclear magnetic resonance spectroscopy (NOESY NMR). The electrospun fibers of this blend under a low take-up velocity (below 310 m/min) show not only microdomain orientation but also (i) the fragmented lamellar grains which orient almost perfectly parallel to the stretching direction (SD) or fiber axis, and (ii) the lamellar angles (μ) are also almost parallel to the fiber axis. When the take-up velocity reaches a certain level (~620 and 1240 m/min), the extensional force overcomes the $\pi-\pi$ interaction between SEBS and BZ, and as a result, the regular microdomains oriented to the fiber axis are suddenly diminished. Thermal treatment of the fibers (~170 °C) initiates the lamellar microdomain rearrangement to an isotropic one with significant traces of lamellar orientation parallel and perpendicular to the fiber axis. The present work demonstrates how two extreme combined conditions, which are (i) macroscopic external stimulus, i.e., extensional force, and (ii) specific interaction at molecular level, i.e., $\pi-\pi$ interaction, direct the orientation of microdomains in the confined space of the as-spun electrospun fibers to be a uniaxial microdomain aligned parallel to the fiber axis.

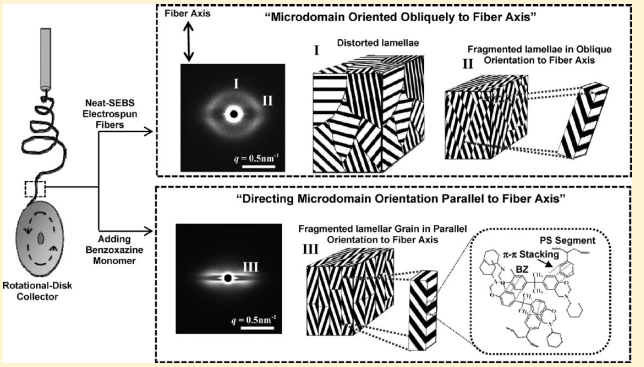

INTRODUCTION

Block copolymers are polymeric materials which have been extensively studied for decades due to the synergistic unique properties, such as the toughness, stiffness and chemical resistance of the different homopolymers.[1−3] Morphologically, block copolymers spontaneously undergo nanophase separation because of the immiscibility of each block. Upon this phase separation, block copolymers form regularly ordered microdomains, such as spheres,[4] cylinders,[5,6] gyroids,[7] and lamellae.[8] Each microdomain in the nanometer scale forms a superlattice structure within the grain which sometimes is in excess of tens of micrometers. The unique morphologies play an important role in internal-reinforcement and contribute directly to the macroscopic properties of the materials.[9] Various techniques, such as annealing,[10] applying external force[11,12] and placing in an electric-field,[13] have been reported as tools to control the microdomain orientation, an unification of microdomain grains, etc.

Electrospinning is known as a versatile technique for fabricating ultrafine fiber in the nanometer scale to a few micrometers. Electric force is used to draw the fluid jet from the needle in a millisecond time scale. In other words, the fluid jet is pulled toward the collector at extremely high stress, and solidified into nano- or microfibers.[14] Thus, electrospinning is an excellent technique for controlling microdomain orientation and arrangement since not only does the technique give an extremely high stress to the block copolymer fluid but also it rearranges the microdomain structure in a confined geometry. Fong and Reneker reported nanophase separation of polystyrene-*block*-polybutadiene-*block*-polystyrene triblock copolymer (SBS) in the electrospun fibers.[15] However, only ill-developed, small,

Received: July 27, 2011
Revised: September 28, 2011
Published: November 10, 2011

Scheme 1

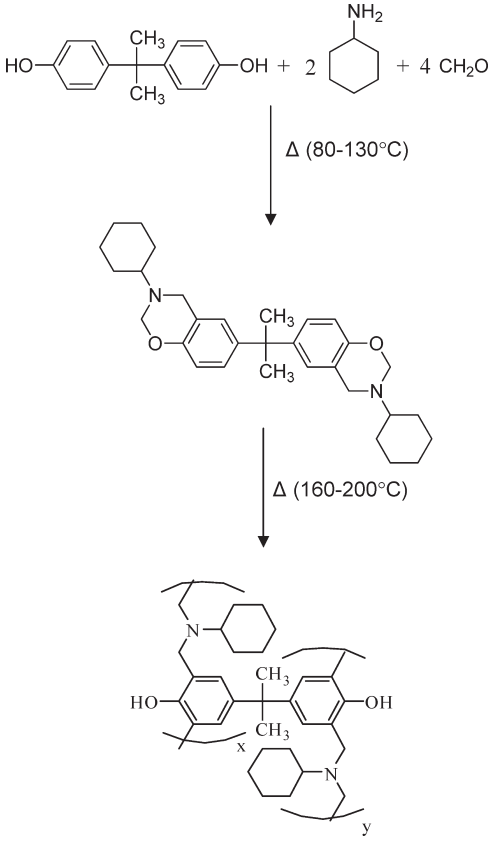

and peculiar shaped microdomains in the SBS as-spun electrospining fibers were investigated. A rapid evaporation of solvent might freeze the polymer chain resulting in segregation into thermodynamically unstable microdomains.[10,15−17]

Recently, we revealed for the first time an existence of a well-ordered and oriented microdomains in the as-spun electrospinning fibers of block copolymer through the study case of SEBS.[18] The evidence of elliptic and four-spot 2D-SAXS patterns has led us to the speculation that, after the microdomains were formed, they might be deformed by electric force during the spinning resulting in the distorted and fragmented microdomains with a preferential orientation to the fiber axis. We were surprised to see that instead of the high take-up velocity (1240 m/min), the lower one (31.5 m/min) significantly induced microdomain distortion. We speculate that the low take-up velocities might allow more time for solvent evaporation and vitrification of PS microdomains and, as a result, not only the existence of microdomain orientation but also a certain level of orientation parallel to the fiber axis could be generated. In addition, the vitrified glassy PS plays an important role in allowing effective stretching resulting in a ductile fracture and a distorted lamellar structure in some cases.

Molecular self-assembly via molecular interaction, such as hydrogen bonding,[19] stereocomplexation[20] and electrostatic interaction,[21] has been well-known for controlling polymer morphologies and properties. In the case of nanofiber, Liu et al. reported the control of the morphology of poly(ethylene oxide) (PEO) electrospun nanofiber by adding thiourea which can form complex with ethylene oxide unit in PEO chain via hydrogen bonding. They revealed that the crystalline phase of thiourea−PEO complex showed the lamellar morphology with highly preferential orientation paralleled to the fiber axis. This hints us that, in our case, the molecular self-assembly with specific interaction might enhance the PS microdomain orientation or, at least, improve the vitrification of those microdomains for effectively response to the extensional or stretching force.[19]

Polybenzoxazines (polyBZ) are a novel type of phenolic resin, which can be prepared from benzoxazine monomers and consequent thermal curing (Scheme 1).[22−27] Recently, we showed a unique in situ nanosphere polyBZ formation in SEBS film matrices.[28] The depth structural analyses brought us to an understanding that initially $\pi-\pi$ interaction was formed between aromatic rings of BZ monomer and styrene blocks in the SEBS chain.

On the basis of the above-mentioned works, how the $\pi-\pi$ interaction between BZ and SEBS plays a role in the morphology of SEBS electrospun fiber comes to our question. The present work is an extension of our previous work where we successfully showed an existence of microdomain orientation in electrospun thermoplastic elastomer SEBS. Here, we further focus on electrospun SEBS blended with BZ (SEBS-BZ) under two extreme combined conditions which are macroscopic the level of electrospinning condition, i.e., stretching force, and molecular level of specific interaction, i.e., the $\pi-\pi$ interaction between SEBS and BZ to study how the microdomains of SEBS respond to those conditions, especially when the SEBS are in the form of electrospun in a confined space.

EXPERIMENTAL SECTION

Materials. SEBS triblock copolymer with 32 wt % styrene content, M_w of 77 000 g/mol, and M_n of 60 000 with PDI of 1.28, measured by GPC, was provided by Asahi Kasei Chemicals Cooperation, Japan. Bisphenol-A, paraformaldehyde and cyclohexylamine were purchased from Fluka, Switzerland. Chloroform and toluene were purchased from Nacalai Tesque, Inc., Japan. All chemicals were used without further purification.

Synthesis of Benzoxazine Monomer (BZ). 6,6′-(propane-2,2-diyl)bis(3-cyclohexyl-3,4-dihydro-2*H*-benzo[*e*][1,3]oxazine) was synthesized (Scheme 1) from bisphenol A, formaldehyde, and cyclohexlamine by mixing and stirring at about 110 °C for 30 min as reported elsewhere.[20]

Preparation of SEBS-BZ Blending Electrospun Fibers. SEBS and BZ were mixed in a weight ratio (w/w) of 75:25 (S75BZ25). The mixture was dissolved in a mixed solvent of chloroform/toluene (80/20 wt/wt). The homogeneous solution obtained was electrospun using a Nanon Electrospinning Setup (MECC Co., Ltd., Japan) equipped with an originally designed rotational disk collector. The optimal spinning conditions were as follows: accelerated voltage, 20 kV; volumetric flow rate, 0.5 mL/h; and, tip-to-collector distance, 15 cm. The fibers were collected onto a rotational disk collector with controllable take-up velocity (i.e., 31.5, 310, 620, and 1240 m/min). The relative humidity for spinning was in the range 30−32%.

Characterization. Two-dimensional nuclear magnetic resonance (2D-NMR) in nuclear overhauser effect spectroscopy (NOESY) mode was conducted by an NMR Bruker Ultrashield Plus 500 MHz at room temperature with a mixing time of 0.4 s. The fiber morphology was observed by a JEOL JSM-5200 scanning electron microscope, and the average fiber diameter was determined by Image J software. 2D-SAXS measurements were carried out at the RIKEN structural biology beamline I (BL45XU) SPring-8, Hyogo, Japan. The 2D-SAXS patterns were recorded using a RIGAKU R-AXIS IV++ equipped with an imaging plate detector (300 mm × 300 mm area). The X-ray wavelength, λ, was tuned at λ = 0.10 nm, and the q value, defined by $q = (4\pi/\lambda)\sin(\theta/2)$ (θ: the scattering angle), was calibrated by chicken tendon collagen having a

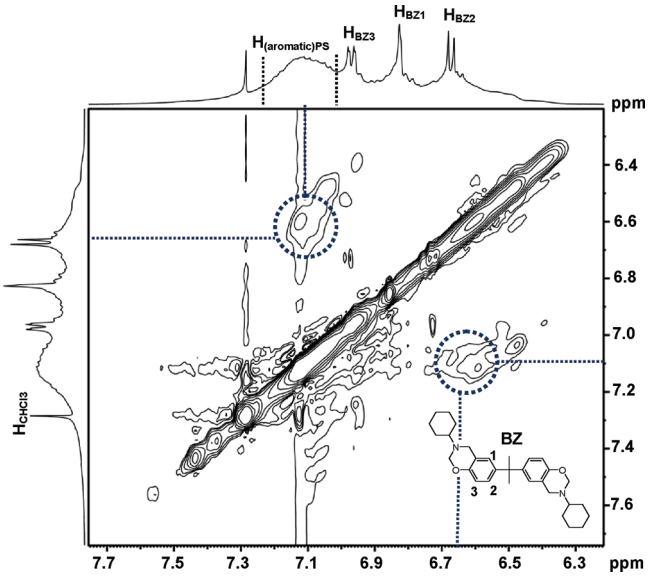

Figure 1. 2D-NMR NOESY contour plot of S50BZ50 in $CDCl_3$ at the concentration of 3.9 × 10^{-3}% w/w.

spacing of 65.3 nm. The viscosity of the spinning solutions was measured by a Brookfield viscometer (Model DVIII, Brookfield Engineering Laboratories INC., Stoughton, MA) with the temperature control at 28 °C. The viscosity of diluted SEBS-BZ blends was measured by a CANNON Ubbelohde 50 B582 with a CANNON CT1000 constant temperature bath at 30 °C.

RESULTS AND DISCUSSION

$\pi-\pi$ Interaction between BZ and PS Block in SEBS. Figure 1 shows a 2D-NMR NOESY contour of S75BZ25 in $CDCl_3$. The aromatic protons of BZ are seen clearly at the chemical shifts of 6.97, 6.82, and 6.68 ppm which contribute to the aromatic protons of BZ in the positions of 3, 1, and 2, respectively. The proton resonance of PS can be observed as a broad peak in the range of 6.97−7.24 ppm. The NOESY contour clearly shows a correlation between the aromatic proton of BZ at position 2(H_{BZ2}) and that of PS in SEBS. This implies $\pi-\pi$ interaction which might be formed either by a charge transfer between electron-rich and electron-poor aromatic compounds[29,30] or by a local dipole of charge distribution in identical-electronic aromatic compounds.[31,32] The latter may be appropriate to our case since both aromatic rings in the BZ and in the PS block are of electron-rich type.

The viscosity of the spinning solution was found to increase significantly, for example, from 1449 cP (±4 cP) for SEBS to 1743 cP (±3 cP) for S75BZ25 under the same concentration of 18 wt %. The fact that the mixture showed an increase in viscosity in spite of the actual concentration of SEBS being diluted by adding BZ for 25 wt %. Furthermore, to clarify this in detail, Ubbelohde capillary viscometer was used to measure the viscosities of the SEBS-BZ blends in dilute condition (1 wt % of SEBS-BZ blend in 80:20/chloroform:toluene). The results showed an increase of specific viscosity (η_{sp}) as the BZ content was increased, which are 3.39 (±0.01), 3.47 (±0.02), 3.50 (±0.03), and 4.27 (±0.04), for SEBS: BZ (wt %) for 100:0, 25:75, 50:50, and 75:25, respectively. This implied the interaction between SEBS and BZ, which might be $\pi-\pi$ interaction as shown in Scheme 2.

Microdomain Structure in SEBS and S75BZ25 Films. In order to investigate the structural change in the microdomain

Scheme 2

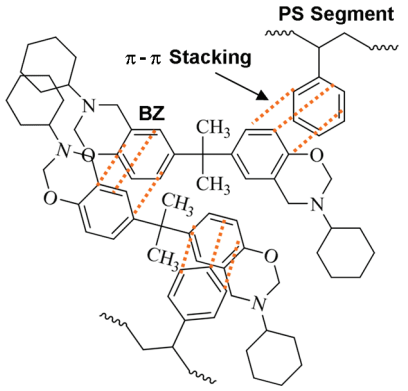

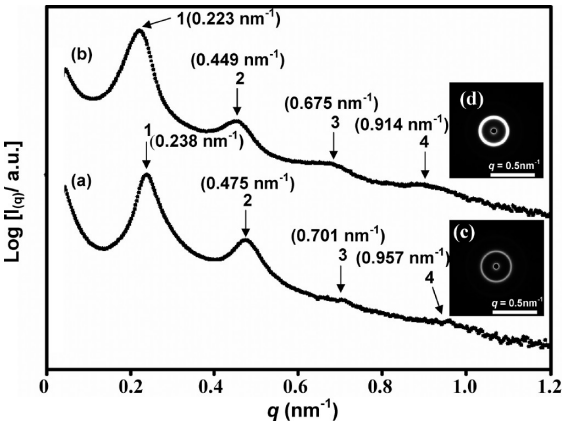

Figure 2. Circular average SAXS profiles: (a) SEBS film, and (b) S75BZ25 film. 2D-SAXS patterns: (c) SEBS film, and (d) S75BZ25 film.

structure for the as-spun fibers, their morphology should first be clarified. As-cast film SEBS was characterized by 2D-SAXS finding that the SAXS profile shows a series of scattering maxima at relative q positions of 1: 2: 3: 4 suggesting a lamellar morphology of the microdomains (Figure 2a-b). For S75BZ25 film (Figure 2b), it shows a series of scattering maxima at relative q positions similar to those of the as-cast SEBS film indicating lamellar-microdomain structures. Furthermore, the circular patterns (Figure 2c-d) indicate no preferential orientation of lamellar microdomains in both as-cast SEBS and S75BZ25 films. It should be noted that the S75BZ25 film shows a slight decrease of each q peak position. This indicates that there is a slight increase in the lamellar repeating period, as compared to the SEBS film. The increase in the lamellar period might be accounted for by the occupation of BZ in PS lamellar microdomains.

Microdomain Arrangement and Orientation in As-Spun SEBS Fibers. The optimal electrospinning parameters were preliminary studied to find the conditions as follows; accelerated voltage at 20 kV, and 18 wt % solid content of SEBS in the mixed solvent (80:20/chloroform: toluene). In order to investigate the effect of the extensional force to microdomain arrangement and orientation in SEBS electrospun fibers, the velocity of the rotational disk collector was varied from 31.5 to 1240 m/min.

Figure 3 shows the appearance and size of the fibers as observed by SEM. The plots of fiber diameters indicate clearly

dx.doi.org/10.1021/ma2017315 |Macromolecules 2011, 44, 9276–9285

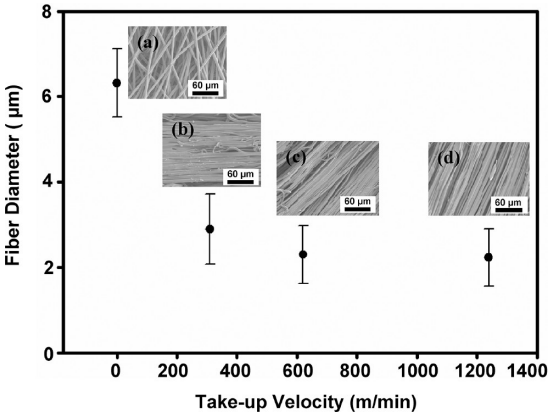

Figure 3. Average diameters and SEM images of the as-spun S75BZ25 electrospinning fibers at various take-up velocities: (a) 31.5 m/min; (b) 310 m/min; (c and d) for those fibers collected at 620 and 1240 m/min, respectively.

how the take-up velocity significantly reduced the fiber diameter. The minimal diameter of the fibers obtained from the take-up velocity at 620 m/min and 1240 m/min is about 2.5 μm. This suggests that the high stretching force initiated by the high take-up velocity of the rotational disk collector led to a decrease in fiber diameters. As discussed in our previous work, the viscoelasticity and low conductivity of the spinning solution limited the fiber diameter so it was smaller than 1 μm.

Previously, we had already clarified an existence of short-range order lamellar microdomains and their orientation.[18] Here, detailed analyses relevant to the fiber take-up velocity of SEBS microdomains was done.

Figure 4 aims for a simple illustration of the morphologies containing different microdomains as the information from 2D-SAXS patterns. The broad scattering peak as a consequence of the deviation of the microdomains in real space, such as finite grain size, lamellar repeating period and imperfect microdomain ordering were omitted. Figure 4a and b summarize the 2D-SAXS patterns of the SEBS electrospun which show the elliptic peak and four streak-like peak patterns. The elliptic peak indicates anisotropic deformation as a result of stretching during spinning along the fiber axis, whereas the four-point pattern is ascribed to glassy lamellar microdomains which are ruptured to tiny fragments, or a so-called herringbone structure.[33] It should be emphasized that the four streak-like peaks were aligned obliquely to the stretching direction (SD).[9,34] Also it should be noted that the fibers collected at the lowest (31.5 m/min) take-up velocity show the most distorted elliptic peak position of the 2D-SAXS pattern. This unexpected result might be the vitrification of PS microdomains took place during spinning. In other words, the time can be determined by a balance of the solvent evaporation rate and the take-up velocity.[18] As shown in Figure 4c, a stretching of the fiber with vitrified PS microdomains might lead to a highly anisotropic deformation. It is important to note that Figure 4 aims for a simply illustration of the morphologies containing different microdomains as the information from 2D-SAXS patterns. The broad scattering peak as a consequence of the deviation of the microdomains in real space, such as finite grain size, lamellar repeating period and imperfect microdomain ordering were omitted.

Effect of BZ to Microdomains in As-Spun SEBS Fibers. As BZ forms a kind of physical cross-link with PS segments in the SEBS chain via $\pi-\pi$ interaction, it leads us to question how this physical cross-link initiates the change in microdomain morphology. The changes of microdomains in the as-spun electrospinning SEBS fibers under the effect of BZ can be traced by the 2D-SAXS patterns. Here, to simplify the study, only the SEBS blend with BZ for 25 wt % content (S75BZ25) was considered as a representative condition.

The structural change of the microdomains in as-spun SEBS and S75BZ25 fibers upon the increase of take-up velocity was qualitatively analyzed as follows. The as-spun SEBS shows dark streaks along the equatorial direction (Figure 4a). The as-spun S75BZ25 fibers obtained from any take-up velocity also show dark streaks (Figure 4d,g,j,m) similar to the case of the as-spun SEBS. This indicates a lack of the large-distance lamellar stacking parallel to the fiber axis which was discussed in our previous work.[18] With careful observation of the scattering patterns of the as-spun SEBS, one can see pattern I (elliptical pattern) and pattern II (four-spot or four-streak pattern) as quoted in Figure 4b. The elliptical pattern reflects an anisotropic deformation upon the stretching as simplified in Figure 4f whereas the four-spot pattern refers to a fragmented lamellar structure as illustrated in Figure 4c.

In the case of S75BZ25 fiber collected at the lowest take-up velocity, i.e. 31.5 m/min, both elliptical and four-spot patterns are identified (Figure 4d). It is important to note that the angle ϕ of the four-spot peak is 90° to the fiber axis. This indicates that the lamellar grains are oriented parallel to the SD. When the stretching was varied by increasing the take-up velocity, for example to 310 m/min, the four-spot pattern became obvious and the elliptical peak was diminished. This implies that at this level of the stress, the large lamellar grains are ruptured in to tiny ones and the lamellae are oriented obliquely to the stretching direction which is known as the herringbone structure as schematically shown in Figure 4c,i.

Taking the above results into consideration, we suspect the microdomain formation of S75BZ25 as follows. On the basis of the physical cross-link between BZ and PS block in SEBS chains through $\pi-\pi$ interaction, the PS microdomains might be considered to be more or less vitrified after solidification. Such vitrified PS microdomains are very responsive to the external force, i.e., stretching force from the rotational disk collector. This resulted in a significant microdomain orientation which never appeared in the neat SEBS fiber case.

In order to characterize the herringbone structure in detail, five parameters from 2D-SAXS patterns were evaluated (Figure 4b,e).[18,34] As imperfection in symmetry may cause some differences in each streak-like spot, each parameter was averaged to obtain a representative value. For fibers collected at take-up velocities of 31.5 and 310 m/min, as illustrated in Figure 4e,h, the four streaks are parallel to each other and perpendicular to the fiber axis as in pattern III. The pattern III refers to anisotropic grains oriented longitudinally parallel to the fiber axis as schematically drawn in detail in Figure 4i. The widths of the streak in the perpendicular and in the parallel directions to the fiber axis are referred to as σ and δ, respectively, as indicated in Figure 4d,e. These parameters are inversely proportional to the grain size in the directions perpendicular and parallel to the fiber axis, respectively, which are also shown in Figure 4i. The angle ϕ is an oblique angle of the streak respected to the fiber axis and μ is an angle of the q vector pointing to the peak maximum respected to the fiber axis (Figure 4b,e). According to the herringbone structure, ϕ and μ correspond to the angle of the normal vector of

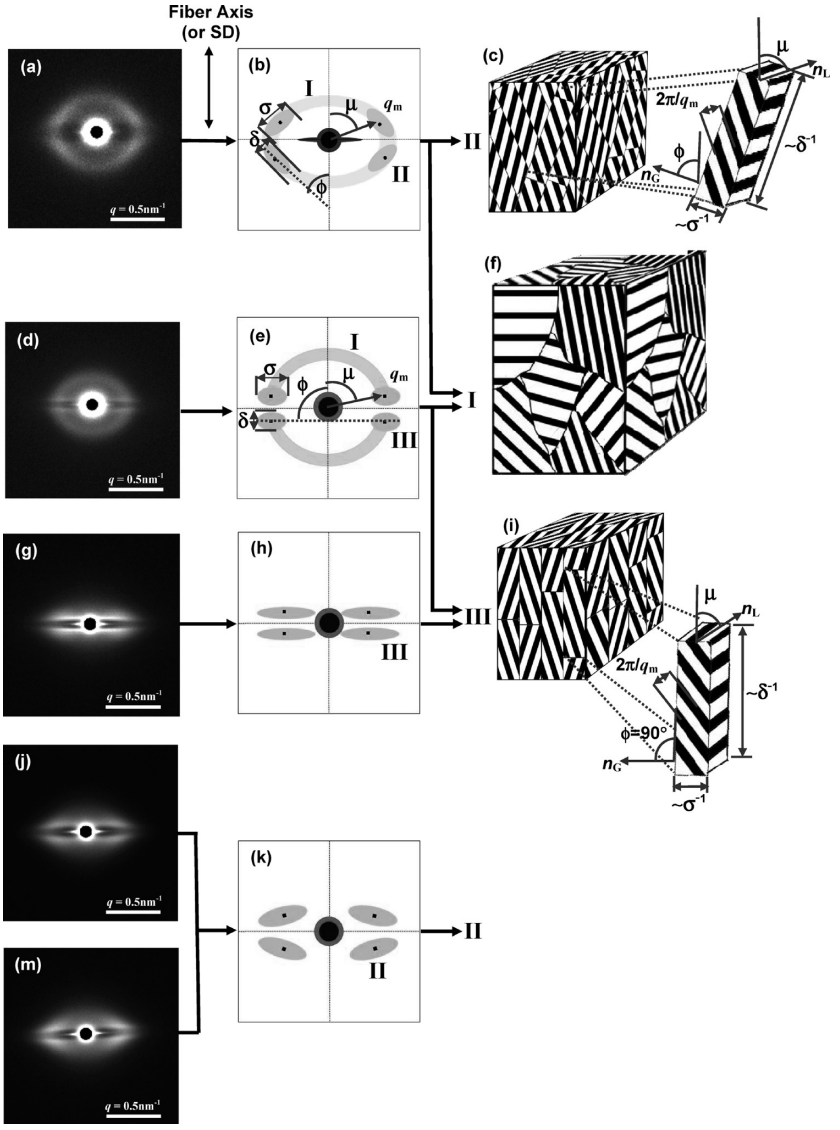

Figure 4. 2D-SAXS patterns: (a) as-spun SEBS electrospining fibers collected at 310 m/min and as-spun S75BZ25 electrospinning fibers collected at (d) 31.5, (g) 310, (j) 620, and (m) 1240 m/min. Schematic illustrations highlighting the features of the 2D-SAXS patterns: (b) for a, (e) for d, (h) for g, and k for (j and m). Possible models: (c) for oblique-herringbone I, (f) for distorted-lamellar II, and (i) for parallel-herringbone III.

the grain, n_G, and that of the lamellar microdomain, n_L, with respect to the fiber axis, respectively (Figure 4c,i). The magnitude of the q vector at the peak maximum is denoted as q_m, which is inversely proportional to the lamellar repeating period. For the fibers collected at 620 and 1240 m/min, the four streaks are obliquely oriented to the fiber axis (Figure 4j,m) and this can be schematically shown as Figure 4k (pattern II).

Microdomain Parameters. Parts c and i of Figure 4 contain important information for the quantitative analysis of microdomain orientation. Here, each parameter, i.e., lamellar repeating period ($2\pi/q_m$), grain dimension (δ^{-1}, and σ^{-1}), grain tilt angle (ϕ), and lamellar tilt angle (μ), can be evaluated.

For the lamellar repeating period of SEBS fibers (Figure 5A), the values are almost constant (about 17−18 nm) although they were obtained from the different take-up velocities. In the case of S75BZ25, the lamellar repeating periods are about 19−22 nm which are larger than those of SEBS. The S75BZ25 fiber obtained from the take-up velocity 310 m/min shows the highest lamellar repeating period. Since this take-up velocity gives the most microdomain orientation parallel to the fiber axis, this velocity can be considered as a critical velocity when the $\pi-\pi$ interaction is still maintained. (further discussion in Figure 5B,C).

The σ and δ (Figure 5B) are the values relevant to grain dimension. For comparative information, the σ and δ values, which can be roughly approximated to be the width and length based on $2\pi/q$, were considered. In the case of SEBS, the grain dimension based on σ values (0.28−0.34 nm^{-1}) and δ values (0.09−0.12 nm^{-1}) the width and length of the grains are estimated to be 18−20 nm and 51−75 nm, respectively. Figure 5B shows that both σ and δ values are decreased as the take-up velocity increased and are constant at high take-up velocities (above 310 m/min). This indicates that by increasing the take-up velocity, the grain dimension might be stretched in the SD direction and this result in an increase of the width and the length of the microdomain grain.

dx.doi.org/10.1021/ma2017315 |*Macromolecules* 2011, 44, 9276–9285

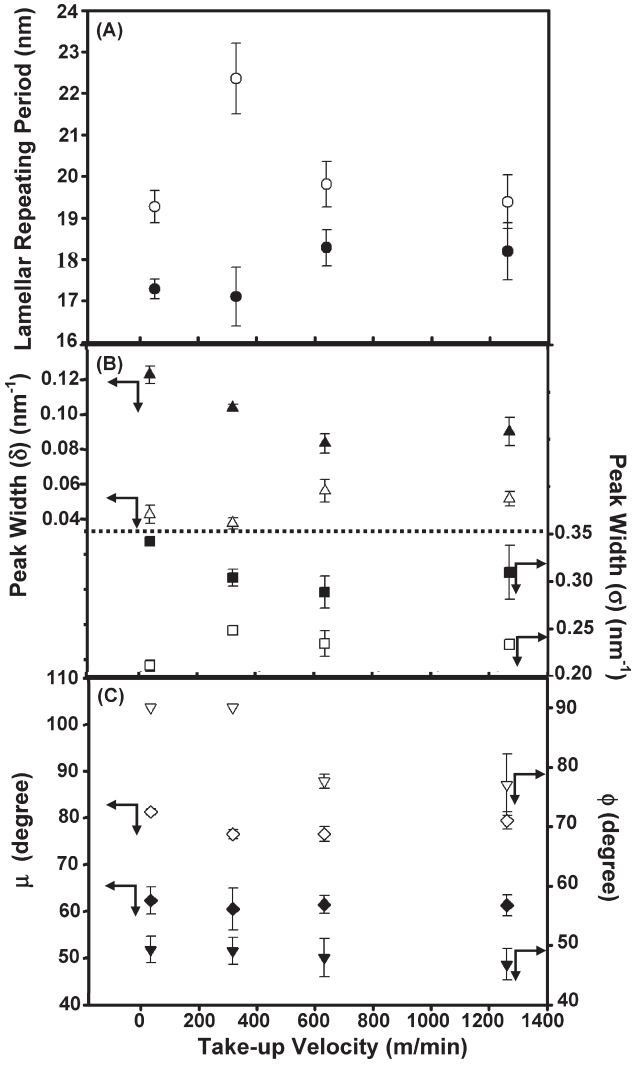

Figure 5. Structural parameters of the as-spun electrospinning fibers collected at various take-up velocities: (A) lamellar repeating periods of SEBS (●) and S75BZ25 (○); (B) peak width parameters σ and δ of SEBS (■ and ▲) and S75BZ25 (□ and △); (C) angle parameters μ and ϕ of SEBS (♦ and ▼), and S75BZ25 (◇ and ▽).

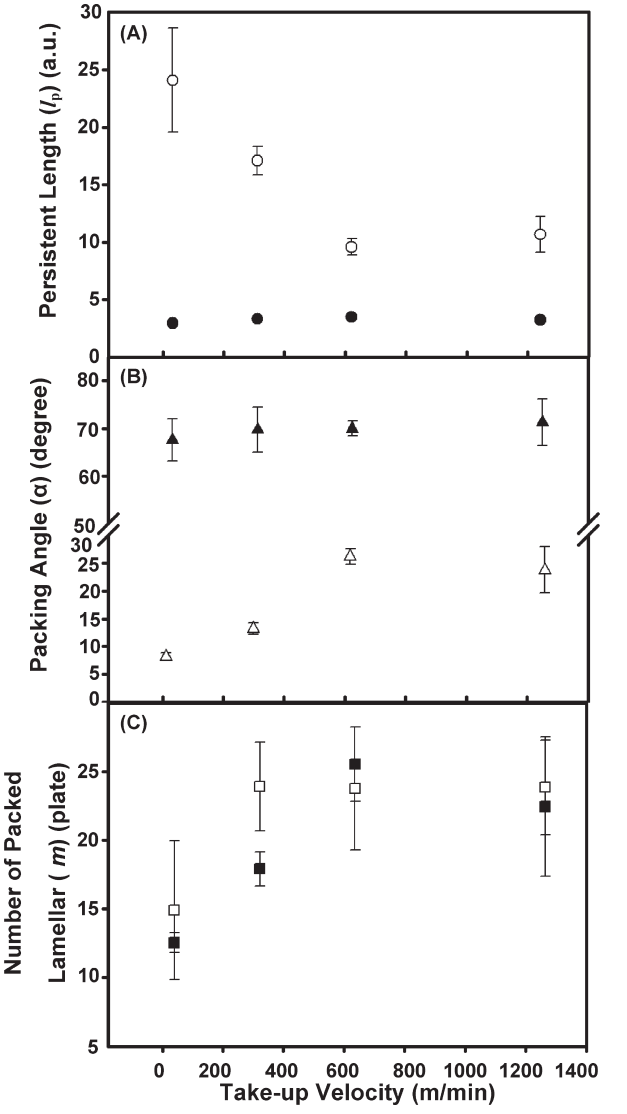

Figure 6. Individual grain parameters of the as-spun electrospinning fibers collected at various take-up velocities: (A) persistent length of the fragmented lamellae (l_p) of SEBS (●) and S75BZ25 (○); (B) packing angle (α) of SEBS (▲) and S75BZ25 (△); (C) number of the packed lamellae in the grain (m) of SEBS (■) and S75BZ25 (□).

In the case of S75B25, the σ values (0.21−0.25 nm^{-1}) and δ values (0.04−0.05 nm^{-1}) give the width and length of the grain about 25−30 nm and 111−166 nm, respectively (Figure 5B). The take-up velocities at 310 m/min initiate the length of the grain to be the highest which is 166 nm. This implies that (i) the take-up velocity did not show effects on the width (σ) as much as on the length (δ) and that (ii) a certain level of the take-up velocity initiated the longest grain of lamellae.

It is important to note that both parameters, σ and δ, of S75BZ25 are smaller than those of the as-spun SEBS. This means that the lamellar grains of S75BZ25 are relatively larger than those of the as-spun SEBS. The reason might be related to the more vitrified microdomains under the $\pi-\pi$ bonded network between BZ and PS segments in SEBS.

The ϕ and μ values allow us to consider how the lamellar grains and microdomains are oriented to the SD. In Figure 5C, the ϕ values of SEBS fibers are about 50° for all take-up velocities whereas those of S75BZ25 are varied. The take-up velocities at 31.5 and 310 m/min give the ϕ values most close to 90°. This indicates a parallel direction of lamellar grains to the SD. The ϕ values abruptly drop to 78° when the take-up velocity is above 310 m/min. For μ values, those of SEBS are maintained at about 60° whereas those of S75B25 are maintained at about 80°. It should be noted that the μ and ϕ values of S75BZ25 are higher than those of SEBS fibers for all take-up velocities. As a conclusion, the S75BZ25 shows the lamellar microdomains and microdomain grains in parallel to the fiber axis or SD as compared to the SEBS fibers.

Corresponding to those parameter changes upon the increase in the take-up velocity (in other words, an increase in the stretching force) the changes of the microdomains in the real space can be considered as follows. In the case of S75BS25 fibers, at low take-up velocity, i.e., 31.5 m/min, the internal structures were stretched resulting in an anisotropic deformation and some parts were fractured into fragmented-lamellar grains and the

dx.doi.org/10.1021/ma2017315 |*Macromolecules* 2011, 44, 9276–9285

orientation parallel to the SD. As the stretching force was increased, the fragmented grains were fractured into more tiny ones but still kept the parallel orientation as evidenced from ϕ being equal to 90° for the take-up velocity at 310 m/min.

To examine the individual grain more concretely, the other three parameters, i.e., persistence length of the fragmented lamellae (l_p), packing angle (α), and number of the packed lamellae in the grain (m) (Figure 6) were considered. Their geometrical definitions are expressed as the following equations.[34]

$$l_p = k\left[\sigma \cos\left(\mu + \phi - \frac{\pi}{2}\right)^{-1}\right] \quad \text{for } \alpha \geq \tan^{-1}(\delta/\sigma) \tag{1}$$

$$l_p = k\left[\partial \sin\left(\mu + \phi - \frac{\pi}{2}\right)^{-1}\right] \quad \text{for } \alpha < \tan^{-1}(\delta/\sigma)$$

(k is an arbitrary constant) (2)

with

$$\alpha = \pi - (\mu + \phi) \tag{3}$$

and

$$m = kq_m(\sigma^{-2} + \delta^{-2})^{1/2} \cos\left[\alpha + \tan^{-1}\left(\frac{\delta}{\sigma}\right) - \frac{\pi}{2}\right] \tag{4}$$

To simplify the calculation, k is assumed to be unity, and the calculated parameters are shown in Figure 6. In the case of SEBS fibers, both l_p and α values are constant for all take-up velocities. For S75B25 fibers, the l_p values are about 9−24 nm which are 3−8 times larger than those of the SEBS. It is important to note that the l_p values are significantly large at the low take-up velocity until 310 m/min and decrease afterward. In contrast, the α values are small at the low take-up velocity and increased with an increase in the take-up velocity. The α values of S75BZ25 fibers are smaller than those of SEBS fibers in all take-up velocities suggesting that the lamellar interface is more or less parallel to the longitudinal-axis direction of the lamellar grains in S75BZ25 fibers as compared to the SEBS fibers. Figure 6D shows concrete images regarding l_p and α values. Therefore, the result of a large l_p with a small α indicates the grain of S75BZ25 consisting of the very long but little tilted lamellae.

Figure 6C shows that the number of the packed lamellae in the case of S75BZ25 is relatively higher than those of SEBS, and is significant at the low take-up velocities, i.e., 31.5 and 310 m/min. This is due to larger grain dimension of S75BZ25 comparing with that of SEBS, especially at the low take-up velocities.

Critical Level of Molecular Interaction in Responsive to Fiber Stretching. Here, another important point is clarified. As illustrated in Scheme 2, the $\pi-\pi$ interaction plays an important role in forming the physical cross-link network between SEBS and BZ. It raises the question that at what level the stretching force overcomes the $\pi-\pi$ interaction. As the stretching force could be controlled by the fiber take-up velocity, the velocity was further increased to observe the change of microdomain structure. Parts j and m of Figure 4 show that when the S75BZ25 fibers were collected at the velocities of 620 and 1240 m/min, the oblique four-streak patterns could observed. In other words, the

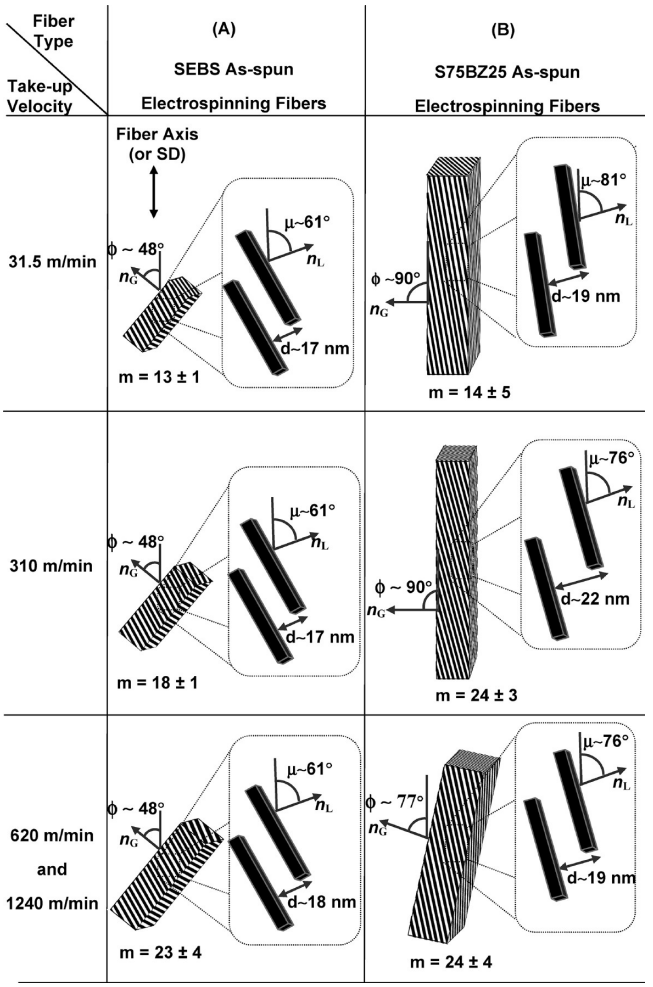

Figure 7. Schematic models summarized from the structural parameters evaluated from 2D-SAXS patterns (Figures 4−6) of lamellar microdomain orientation in the individual grain of the as-spun SEBS and S75BZ25 electrospinning fibers at various take-up velocities.

2D-SAXS patterns become similar to that in the as-spun SEBS fibers (Figure 4a).

Figure 5 also confirms how the applied force obtained from the high take-up velocities, i.e., 620 and 1240 m/min affects the physical bond network between BZ and SEBS. For example, the lamellar repeating period, the δ and σ values become close to those of SEBS when the take-up velocities are 620 and 1240 m/min. In fact, at those velocities, the angles ϕ also disrupt from 90° suggesting an oblique disorientation of the lamellar grain with respect to the fiber axis (Figure 4c).

Comparison of Microdomain Orientation between SEBS and S75BZ25. To simplify the results and make a comparison of microdomain orientation, a series of models highlighting a single grain of microdomains for SEBS[18] and S75BZ25 are illustrated based on 2D-SAXS results (Figure 7). It should be noted that it is difficult to draw the schematic model of the microdomain grain to exactly represent the one in the real space with the fluctuation of the parameters (q_m, δ, σ, μ, ϕ, m, l_p and α) as a consequence of various grains combination. Herein, we simplify the scheme based on gathering of microdomain grains without consideration of those fluctuations. In this way, we can show the effect of BZ and take-up velocity to the microdomain

structure. Figure 7 was drawn up based on the average value of each parameter.

In our previous work,[18] we revealed an existence of the microdomain orientation of SEBS. It should be emphasized, however, that the take-up velocity rarely affects the grain orientations. As seen in Figure 7 (column A), all conditions show a similar grain orientation, ϕ for ~48°, the lamellar repeating period for ~17 nm, and the lamellar angle, μ for ~60°. It should be noted that the number of lamellae included in grain, m, increases with an increase in the take-up velocity as a consequence of the longer grains. When it comes to the cases of S75B25 (Figure 7, column B), it is clear that not only the BZ promotes the microdomain orientation to be parallel to the fiber axis, but also the take-up velocity plays an important role to adjust the details of orientation of the grains and lamellae. For example, in the cases of S75BZ25 fibers collected at 31.5 and 310 m/min, the stretching initiated a preferential orientation of the grain to be parallel to the fiber axis (ϕ = 90°) whereas the orientation angle of the normal vector of lamellae (n_L), μ, were in the range of 75−80° (almost parallel orientation of lamellar plates to SD). For the take-up velocities at 620 and 1240 m/min, the grains tilt a bit (ϕ = ~77°), whereas μ and d were unchanged. Similarly, m increases with an increase of the take-up velocities. It seems that there is a boundary between 310 and 620 m/min of the take-up velocity. In other words, (i) the optimal take-up velocity to promote microdomain orientation of S75BZ25 fibers to be parallel to the fiber axis is about 310 m/min, and (ii) at a take-up velocity higher than 310 m/min, the $\pi-\pi$ interaction between SEBS and BZ in S75B25 might be weakened, and as a result, the grains become tilted to the fiber axis.

Rearrangement of Lamellar Microdomains in S75BZ25 Fibers upon Thermal Treatment. Ma et al. and Kalra et al. reported the peculiar shaped microdomains of polystyrene-block-polyisoprene (SIS) electrospun fibers and showed a rearrangement to a long-ranged ordered ones, as observed in film, after a thermal annealing.[8,10,17] In our previous work, we showed that the obliquely oriented lamellar microdomains of the as-spun SEBS electrospun fibers underwent a rearrangement to the randomly oriented lamellae with dually preferential weak orientation, parallel and perpendicular to the SD by thermal annealing.[18] However, it should be noted that the preferential orientation of the long-ranged microdomains was observed only in the fibers collected at high take-up velocities (610 and 1240 m/min). Thus, it comes to the question how the highly oriented lamellar microdomains in the as-spun S75BZ25 fibers rearrange themselves after thermal treatment.

The fibers were fixed by epoxy glue before annealing at 170 °C for 3 h to maintain the fiber structure as the original one. Figure 8A shows 1D-SAXS profiles (circular average from 2D-SAXS patterns) of annealed S75BZ25 fibers including the films of SEBS and S75B25 for comparative discussion. The as-cast SEBS films show the lamellar repeating period of about ~26.6 nm (profile a). The S75BZ25 films before curing show the lamellar repeating period for ~28.1 nm (profile b) which confirms the occupation of BZ in the lamellar microdomains. After this film was cured, the lamellar repeating period decreased to ~24.3 nm (profile c). This suggests a removal of remaining strain by the thermal treatment. In the case of S75B25 fibers (profiles d−f), the lamellar periods of all fibers appear at the same position, i.e., ~21.9 nm. This indicates the tight lamellar period as compared to that of the films.

Figure 8B shows 2D-SAXS patterns for the annealed S75BZ25 fibers which were collected at varied take-up velocities. It is clear

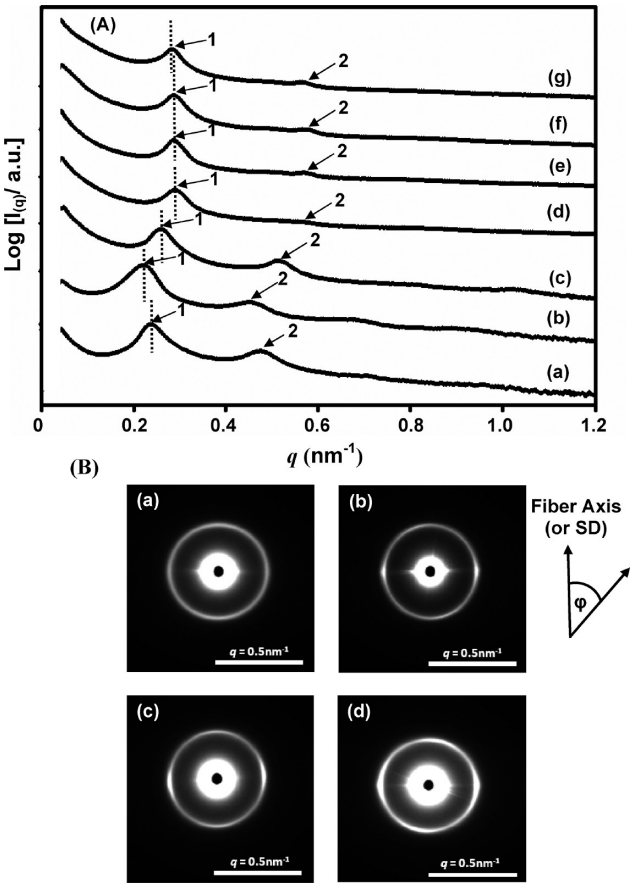

Figure 8. (A) SAXS profiles: (a) as-cast SEBS film, (b) precured S75BZ25 film, (c) postcured S75BZ25 film and postcured S75BZ25 electrospinning fibers collected at (d) 31.5, (e) 310, (f) 620, and (g) 1240 m/min. (B) 2D-SAXS patterns: postcured S75BZ25 electrospinning fibers collected at (a) 31.5, (b) 310, (c) 620, and (d) 1240 m/min. The fibers were fixed in adhesive epoxy before curing at 170 °C for 3 h.

that the microdomain relaxations of all fibers took place resulting in the symmetrically circular 2D-SAXS patterns. This suggests that the fragmented-lamellar microdomains rearrange to a favorable random morphology according to SEBS chain relaxation. Moreover, it should be noted that the preferential orientation of lamellar microdomains after curing is discernible as identified by the intensity accumulation on both equatorial and meridional directions for the first-order peak (shown by arrows in Figure 8B).

To clarify the intensity accumulation, first, the azimuthal angle (φ) in the 2D-SAXS pattern (shown in Figure 8) was defined with respect to the fiber axis (or SD). Therefore, a reflection peak appearing at φ = 0° and 90° was ascribed to the lamellae of which the normal vectors (n_L) are as shown in Figure 9C,D, respectively. The intensity distributions with φ are shown in Figure 9A in which the accumulated intensities in the equatorial direction, i.e., φ = 90° and 270°, and the meridional direction, i.e. φ = 0° and 180°, to the SD are clearly observed. The annealed fibers collected at 310 m/min, 620 m/min, and 1240 m/min, show the significant accumulation of the intensity at $\varphi_{90°,\ 270°}$ rather than those at $\varphi_{0°,\ 360°}$. This indicates that, during the annealing, the strain remaining in the SEBS chains was released. Consequently, it induced a preferential orientation of lamellar microdomains in parallel to the SD. To concretely evaluate

dx.doi.org/10.1021/ma2017315 |Macromolecules 2011, 44, 9276–9285

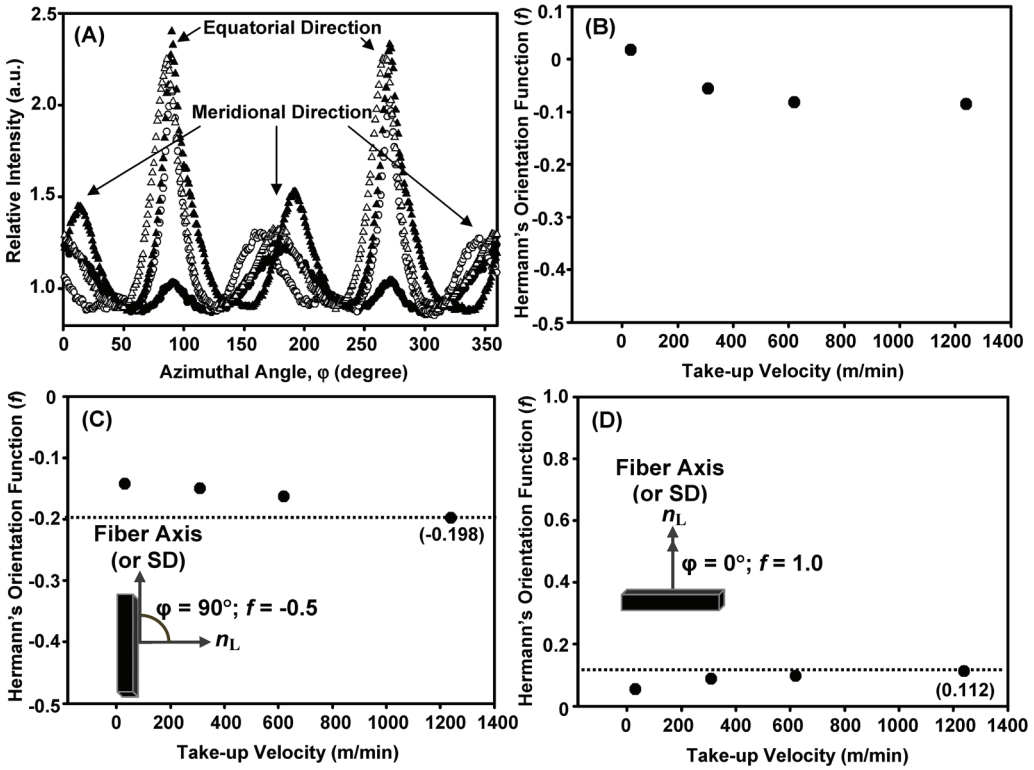

Figure 9. (A) Relative intensity distribution as a function of φ along the first-order peak (azimuthal scan) from 2D-SAXS pattern of annealed S75BZ25 electrospinning fibers collected at (●) 31.5, (○) 310, (▲) 620, and (△) 1240 m/min. Hermann's orientation functions (f) calculated by (B) averaging all scattering directions ($0° < \varphi < 180°$), (C) taking account of equatorial intensity accumulation (after being decomposed) and (D) taking account of meridional intensity accumulation (after being decomposed).

the microdomain orientation, a Hermann's orientation function (f) was calculated according to the following equations:[12]

$$f = \frac{[3\langle\cos^2\varphi\rangle - 1]}{2} \tag{5}$$

$$\text{where } \langle\cos^2\varphi\rangle = \frac{\int_0^{\pi} I_{(\varphi)} \cos^2\varphi \sin\varphi \, d\varphi}{\int_0^{\pi} I_{(\varphi)} \sin\varphi \, d\varphi} \tag{6}$$

The f value is unity in the case of perfectly parallel orientation of n_L to the SD. That is to say, the lamellar plate is perfectly oriented perpendicular to the SD. When the f value is -0.5, the n_L is oriented perfectly perpendicular to the SD. In other words, the lamellar plane is perfectly oriented parallel to the SD. In addition, the f value is zero in the case of random orientation. As shown in Figure 9B, the f values of the annealed fibers were decreased from 0.017 for the take-up velocities of 620 and 1240 m/min to -0.085 for the take-up velocity of 31.5 m/min. This implies the change of the lamellar microdomain orientation (the lamellar plates) from the perpendicular to the SD to the parallel one. It is important to note that, in our case, the patterns show a dual orientation which the conventional calculations of f, representing the average all scattering peaks ($0° < \varphi < 80°$) in eq 6, could not represent the microdomain orientation directly. To analyze this orientation in detail, the peak decomposition technique was applied to obtain four different plots with φ from 0° to 360° corresponding to scattering peak of each azimuthal profile in Figure 9A. Then, the summation of the two decomposed plots with the scattering peaks at $\varphi \sim 0°$ and 180° were summed up to render the single plot with those peaks at $\varphi \sim 0°$ and 180°. Finally, the summed-up plot was used to calculate the f values based on eqs 6 and 5 under the range of $0° < \varphi < 180°$ which are shown in Figure 9C. Similarly, the other two decomposed plots with scattering peaks at $\varphi \sim 90°$ and 270° were used to calculate f values in the same procedure as explained above (see Figure 9D).

The f values for the accumulated intensities of the scattering peaks in the meridional and equatorial directions are in the range of 0.05 to 0.112 and -0.14 to -0.198, respectively, which are quite small as compared to those of the perfectly perpendicular- and parallel-oriented lamellae as schematically drawn in Figure 9D,C, respectively. This indicates that the remaining stress induced only a small number of lamellar microdomains mostly in the parallel to the SD. It is clear that the f value in the equatorial direction became lowest at -0.198 or 39% comparing with f values at -0.5 for the perfectly parallel orientation of lamellar microdomains. Whereas the f values in the meridional direction shows the highest one at 0.112 or 11% compared with the perfectly perpendicular orientation of lamellar microdomains ($f = 1$). This indicates that the applied stress is stored in the SEBS chain, and after the thermal treatment, it causes chain relaxation leading to a rearrangement of microdomains, from short- to long-range ordered ones. At that time, the orientation is under both meridional and parallel to the SD, of which the parallel one is more preferable.

■ CONCLUSIONS

As reported previously,[18] bisphenol A based benzoxazine showed a strong interaction with SEBS via $\pi-\pi$ interaction.

This brought physical-cross-link networks to PS segments in SEBS chains resulting in vitrified PS microdomains. The microdomain orientation of SEBS was responsive to the stress initiated by rotational-disk collector. The present work shows that the velocity of the collector, i.e., take-up velocity, is another key factor to direct the microdomain orientation of SEBS as evidenced from the optimal velocity (310 m/min) leading to a microdomain orientation with a parallel direction to the fiber axis. The velocities above this level were found to initiate the rupture of the physical cross-link network as seen from the change from parallel alignment to obliquely aligned lamellar microdomain orientation. Thermal treatment of SEBS containing BZ not only initiated the curing of BZ to become polyBZ but also annealing SEBS. After thermal treatment, for the fibers, the microdomains became random but with some traces of orientation in parallel and perpendicular to the fiber axis. In addition, for polyBZ, the nanospheres (~180 nm) thermosetting resins can be consequently obtained and this will be reported in our upcoming article. The present work shows a model case to control the microdomain orientation of the electrospun fibers. The SEBS electrospun fiber containing BZ under macroscopic external stretching force along with a specific interaction at molecular level of $\pi-\pi$ interaction between SEBS and BZ proved to us that we could direct the microdomain orientation to be almost perfectly parallel to the fiber axis if there was specific interaction between polymer matrices.

AUTHOR INFORMATION

Corresponding Author

*(S.S.) Telephone: +81-75-724-7864. E-mail: shin@kit.ac.jp. (S.C.) Telephone: +66-2-218-4134. Fax: +66-2-215-4459. E-mail: csuwabun@chula.ac.th. (M.K.) Telephone: +81-75-724-7323. Fax: +81-75-724-7337. E-mail: m-kotaki@kit.ac.jp.

ACKNOWLEDGMENT

S.C. and W.R. would like to express their gratitude to the Thailand Research Fund (the Royal Golden Jubilee Ph.D. Scholarship, Grant No. PHD/0058/2550), Basic Research Grant (BRG-5380010), and the Japan Student Services Organization (JASSO) for financial support. The authors acknowledge Asahi Kasei Chemicals Corporation, Japan, for SEBS. The SAXS experiments were conducted at the SPring-8 with the approved number 2009A1153.

REFERENCES

(1) Holden, G.; Kricheldorf, H. R.; Quirk, R. P. In *Thermoplastic Elastomers*, 3rd ed.; HanserVerlag: Munich, Germany, 2004; pp 2−3.
(2) Bhowmick, A. K.; Stephens, H. L. In *Handbook of Elastomers*, 2nd ed., CRC Press: Boca Raton, FL, 2000; pp 327−330.
(3) Brydson, J. A. *Thermoplastic Elastomers: Properties and Applications*: iSmithers Rapra Publishing: Shawbury, Shrewsbury, Shropshire, U.K., 1995; pp 3−7.
(4) Wang, Y.; Hong, X.; Liu, B.; Ma, C.; Zgang, C. *Macromolecules* **2008**, *41*, 5799–5808.
(5) Heck, B.; Arends, P.; Ganter, M.; Kressler, J.; Stühn, B. *Macromolecules* **1997**, *30*, 4559–4566.
(6) Figueiredo, P.; Geppert, S.; Brandsch, R.; Bar, G.; Thomann, R.; Spontak, R. J.; Gronski, W. *Macromolecules* **2001**, *34*, 71–180.
(7) Shefelbine, T. A.; Vigild, M. E.; Hajduk, D. A.; Hillmyer, M. A.; Cussler, E. L.; Bate, F. S. *J. Am. Chem. Soc.* **1999**, *121* (37), 8457–8465.
(8) Ma, M.; Titievsky, K.; Thomus, E. L.; Rutledge, G. C. *Nano Lett.* **2009**, *9* (4), 1678–1683.
(9) Honeker, C. C.; Thomas, E. L. *Chem. Mater.* **1996**, *8*, 1702–1714.
(10) Kalra, V.; Kakad, P. A.; Mendez, S.; Ivannikov, T.; Kamperman, M.; Joo, Y. L. *Macromolecules* **2006**, *39*, 5453–5457.
(11) Sakurai, S.; Momii, T.; Taie, K.; Shibayama, M.; Nomura, S. *Macromolecules* **1993**, *26*, 485–491.
(12) Sakurai, S.; Aida, S.; Okamoto, S.; Ono, T.; Imaizumi, K.; Nomura, S. *Macromolecules* **2001**, *34*, 3672–3678.
(13) Wang, J. Y.; Chen, W.; Russell, T. P. *Macromolecules* **2008**, *41* (19), 7227–7231.
(14) Ramakrishna, S.; Fujihara, K.;Teo, W. E.;Teo, T. E.; Ma, Z. In *An Introduction to Electrospinning and Nanofibers*: World Scientific Publishing Co. Pte. Ltd.: Singapore, 2005.
(15) Fong, H.; Reneker, D. H. *J. Polym. Sci., B: Polym. Phys* **1999**, *37*, 3488–3493.
(16) Ma, M.; Hill, R. M.; Lowery, J. L.; Fridrikh, S. V.; Rutledge, G. C. *Langmuir*. **2005**, *21*, 5549.
(17) Ma, M.; Krikorian, V.; Yu, J. H.; Thomas, E. L.; Rutledge, G. C. *Nano Lett.* **2006**, *6* (12), 2969–2972.
(18) Rungswang, W.; Kotaki, M.; Sakurai, S.; Shimojima, T.; Kimura, G.; Chirachanchai, S. *Polymer* **2011**, *52*, 844–853.
(19) Lui, Y.; Antaya, H.; Pellerin, C. *J. Phys. Chem. B* **2010**, *114* (7), 2373–2378.
(20) Crne, M.; Park, J. P.; Srinivasarao, M. *Macromolecules* **2009**, *42*, 4353–4355.
(21) Cashion, M. P.; Li, X.; Geng, Y.; Hunley, M. T.; Long, T. E. *Langmuir* **2010**, *26* (2), 678–683.
(22) Ning, X.; Ishida, H. *J. Polym. Sci., B: Polym. Phys* **1994**, *32*, 921–927.
(23) Ishida, H. US Patent 5, 543, 516, 1996.
(24) Ishida, H.; Sanders, D. P. *Macromolecules* **2000**, *33*, 8149–8157.
(25) Takeichi, T.; Agag, T. *High Perform. Polym.* **2006**, *18*, 777–797.
(26) Chaisuwan, T.; Ishida, H. *J. Appl. Polym. Sci.* **2006**, *101*, 548–558.
(27) Agag, T.; Takeichi, T. *Macromolecules* **2003**, *36*, 6010–6017.
(28) Rungswang, W.; Chirachanchai, S. *Macromol. Mater. Eng.* **2011**, *296*, 428–433.
(29) Foster, R. *Chem. Br.* **1976**, *12*, 18.
(30) Reczek, J. J.; Iverson, B. L. *Macromolecules* **2006**, *39*, 5601–5603.
(31) Fisk, C. L.; Becker, E. D.; Miles, H. T.; Pinnavaia, T. J. *J. Am. Chem. Soc.* **1982**, *104*, 3307–3314.
(32) Mo, H.; Pochapsky, T. C. *Prog. Nucl. Magn. Reson. Spectrosc.* **1997**, *30*, 1–38.
(33) Sakurai, S.; Sakamoto, J.; Shibayama, M.; Nomura, S. *Macromolecules* **1993**, *26*, 3351–3356.
(34) Sakurai, S.; Aida, S.; Okamoto, S.; Sakurai, K.; Nomura, S. *Macromolecules* **2003**, *36*, 1930–1939.

NOTE ADDED AFTER ASAP PUBLICATION

This article posted ASAP on November 10, 2011. Equation 3 has been revised. The correct version posted on November 14, 2011.